Journal of Translational Medicine

RESEARCH

Open Access

RPL22L1 fosters malignant features of cervical cancer via the modulation of DUSP6-ERK axis

Dongmei Zhang[1,2,3], Meiqi Zhao[1,2], Ping Jiang[1,2], Yunzhen Zhou[1,2], Xu Yan[1,2], Chong Zhou[1,2], Yu Mu[1,2], Shan Xiao[1,2], Guohua Ji[1,2], Nan Wu[1,2], Donglin Sun[1,2], Xiaobo Cui[1,2], Shangwei Ning[5], Hongxue Meng[6], Sheng Xiao[7] and Yan Jin[1,2,4*]

Abstract

Background Cervical cancer remains one of the leading causes of cancer-related deaths among women globally, and there is still a need to research molecular targets that can be used for prognosis assessment and personalized molecular therapies. Here, we investigate the role of potential molecular target ribosomal L22-like 1 (RPL22L1) on cervical cancer, identify its potential mechanisms, and explore its related applications in prognosis and molecular therapies.

Methods Multiple cervical cancer cohorts online, tissue microarrays and clinical tissue specimens were analyzed for the association between RPL22L1 expression and patient outcomes. Functional and molecular biology studies of cell and mice models were used to clarify the effects and potential mechanisms of RPL22L1 on cervical cancer.

Results RPL22L1 is highly expressed in both cervical adenocarcinoma and squamous cell carcinoma, and its expression is significantly associated with histology grade, clinical stage, recurrence, vascular space involvement, tumor sizes and poor prognosis. In vitro and in vivo experiment revealed that RPL22L1 overexpression significantly promoted cervical cancer cell proliferation, migration, invasion, tumorigenicity and Sorafenib resistance, which were attenuated by RPL22L1 knockdown. Mechanistically, RPL22L1 competitively binds to ERK phosphatase DUSP6, leading to excessive activation of ERK. The combined application of ERK inhibitors can effectively inhibit RPL22L1 overexpressing cervical cancer cells both in vivo and in vitro.

Conclusion RPL22L1 promotes malignant biological behavior of cervical cancer cells by competitively binding with DUSP6, thereby activating the ERK pathway. The combined use of Sorafenib and an ERK inhibitor is a potentially effective molecular targeted therapy for RPL22L1-high cervical cancer.

Keywords RPL22L1, Cervical cancer, ERK, Sorafenib

*Correspondence:
Yan Jin
jinyan@hrbmu.edu.cn
[1]Laboratory of Medical Genetics, Harbin Medical University, Harbin 150081, China
[2]Key Laboratory of Preservation of Human Genetic Resources and Disease Control in China, Harbin Medical University, Harbin 150081, China
[3]Key Laboratory for Molecular Targeted Drug of Heilongjiang Province, College of Pharmacy, Harbin Medical University, Harbin 150081, China
[4]State Key Laboratory of Zone Cardiovascular Diseases in China, Harbin Medical University, Harbin 150081, China
[5]College of Bioinformatics Science and Technology, Harbin Medical University, Harbin 150081, China
[6]Department of Pathology, Harbin Medical University Cancer Hospital, Harbin 150081, China
[7]Department of Pathology, Brigham and Women's Hospital, Harvard Medical School, Boston, MA 02115, USA

Introduction

Cervical cancer is a leading cause of cancer-related mortality among women globally, particularly affecting younger women [1, 2]. The most common histological subtypes are squamous cell carcinomas and adenocarcinomas, which show distinct clinical features and treatment responses due to their different molecular characteristics [3, 4]. Currently, the primary treatments for all cervical cancer subtypes are surgery and chemoradiation, with a lack of effective personalized therapeutic strategies [5–9]. To address this clinical challenge, it is crucial to elucidate the molecular mechanisms underlying cervical cancer and identify more effective biomarkers or targets for targeted therapy.

Increasing evidence highlights the role of the MEK-ERK pathway in the malignant progression of various tumors, including cervical cancer [10–12]. Consequently, targeted therapies that inhibit this pathway, such as Sorafenib and Trametinib, are used as first-line treatments for several cancers, including hepatocellular carcinoma, renal cell carcinoma, thyroid cancer, and melanoma [13–16]. However, resistance to these therapies often develops due to complex mechanisms that affect ERK activation through various pathways [17]. DUSP6, a protein tyrosine phosphatase, plays a crucial role in specifically dephosphorylating ERK, thus providing an important negative control over ERK signaling [18, 19]. Therefore, targeting this negative regulatory mechanism could offer a novel strategy to effectively modulate the MEK-ERK pathway.

Ribosomal proteins are involved in tumor progression, metastasis, and therapeutic resistance [20]. Ribosomal L22-like 1 (RPL22L1), a novel paralog of ribosomal proteins, was identified by our group as an oncogene that contributes to ovarian cancer metastasis by inducing epithelial-to-mesenchymal transition (EMT) [21]. Our further studies have confirmed that RPL22L1 accelerates the malignant progression of hepatocellular carcinoma and glioblastoma, and affects their sensitivity to targeted therapies [22, 23]. RPL22L1 is also associated with the progression of several solid tumors such as colorectal cancer [24], prostate cancer [25], renal cell carcinoma [26] and neuroblastoma [27]. However, its role in cervical cancer has not yet been explored.

In this study, we demonstrate that RPL22L1 is universally highly expressed in cervical cancer and drives tumor malignancy through its competitive interaction with DUSP6, leading to ERK activation. The combined application of ERK inhibitors with Sorafenib can effectively inhibit cervical cancer cells with high RPL22L1 expression both in vivo and in vitro. Therefore, our findings reveal RPL22L1 to be a promising indicator to guide ERK inhibitor combination therapy in cervical cancer.

Materials and methods

Cervical cancer tissue microarrays and clinical specimens

Human cervical cancer tissue microarrays, including F801301 (40 non-tumor, 25 adenocarcinoma, and 15 squamous cell carcinoma) and F1081301 (8 non-tumor, 40 adenocarcinoma, and 60 squamous cell carcinoma), were purchased from Zhong Ke Guang Hua Biotech (Xi'an, China). Additionally, 130 specimens of primary adenocarcinoma patients were collected at the time of diagnosis, prior to any therapy, from Department of Gynecology, Harbin Medical University Cancer Hospital.

Bioinformatics analysis

Genetic alterations of RPL22L1 in cervical cancer were retrieved from cBioPortal (http://www.cbioportal.org). The mRNA expression of RPL22L1 in different cancer types was analyzed using ULCAN cancer database (https://ualcan.path.uab.edu/index.html). RNA-Seq (Counts) and clinical information for the TCGA-CESC cohort were obtained from UCSC Xena (https://xenabrowser.net/datapages/). The "Series Matrix File(s)" for the GSE7410, GSE166466, GSE122697 and GSE146114 datasets were loaded from NCBI GEO database. RPL22L1-related genes were identified from GeneCards. Kinase Target analysis was performed by gene set enrichment analysis (GSEA) and Over-Representation Analysis (ORA) function in LinkedOmics (http://www.linkedomics.org). The interaction network involving RPL22L1 was explored using BioGRID V4.4.240 [28], GeneMANIA [29] and Cytoscape V3.10.3 [30].

Protein-protein docking

AlphaFold 3 (https://alphafoldserver.com/) was used to predict the 3D structures of RPL22L1 and DUSP6 proteins. Schrodinger's Maestro 13.5 software (Schrödinger Inc, New York, USA) was employed to predict the interaction between RPL22L1 and DUSP6. The Protein Preparation Wizard module was applied for protein preprocessing (PH = 7.0 ± 2.0), regeneration of native ligand states, optimization of H-bond assignments, minimization of protein energy, and removal of waters. The protein-protein docking module was utilized to conduct docking with the RPL22L1 and DUSP6 proteins, with the 'Number of ligand rotations to probe' set to 70,000 and 'Maximum poses to return' set to 30. The conformation with the lowest PIPER pose energy was selected for identifying the interaction regions and binding sites. The interaction complex was color-coded for different chains, and added a surface to display the 3D structures. Finally, the Protein Interaction Analysis module was employed to identify the binding regions.

Cell lines and reagents

Human cervical adenocarcinoma cell line HeLa (CCL-2.1 ™) and squamous cell carcinoma cell lines SiHa (HTB-35 ™) and CaSki (CRM-CRL-1550 ™) were purchased from the American Type Culture Collection (ATCC, Manassas, VA). All cell lines were recently STR authenticated at the Micro-read Genetics Company (Beijing, China). Mitomycin C (HY-13316), SCH772984 (HY-50846), Ulixertinib (HY-15816), U0126 (HY-12031 A) and Sorafenib (HY-10201) were obtained from MedChemExpress (NJ, USA).

Immunohistochemistry (IHC)

IHC staining was performed with PowerVision™ Two-Step Histostaining Reagent (Zhongshan Golden Bridge, Beijing, China). Briefly, all slides were dewaxed and blocked. Following overnight incubation with primary antibodies (Supplementary Table 1) at 4 °C, the sections were incubated with goat anti-rabbit IgG for 20 min. The color reaction was completed using diaminobenzidine. Sections were then counterstained with hematoxylin, and photographed.

Isolation of HeLa-I cells with high invasiveness

Highly invasive HeLa-I cells were isolated using transwell chamber precoated with Matrigel. HeLa cells were seeded into the upper chamber with media containing 2% fetal bovine serum (FBS), while media containing 20% FBS was added to the lower chambers. Following 72-hour incubation, cells that had migrated to the lower chamber through the transwell membrane were collected and subsequently cultured for 30 days. This procedure was repeated for 5 cycles to ensure the generation of highly invasive cells, which were then validated using transwell migration and invasion assays.

Cell transfection

Lentiviruses expressing RPL22L1 or vector, as well as those silencing RPL22L1 or negative control, were purchased from HANBio (Shanghai, China). All lentiviruses were transfected into cells using polybrene (HANBio, Shanghai, China) following the manufacturer's instructions. Small interfering RNAs (siRNAs) targeting DUSP6 (siDUSP6-1-3) were synthesized by RiBoBio Co. Ltd (Guangzhou, China), with a scrambled negative control siRNA used as control. Cells were transfected with these siRNAs using X-treme gene HP reagent (Roche, Mannheim, Germany) following the operation manual.

Western blotting

Cells were lysed with RIPA buffer (Thermo Fisher Scientific, MA, USA). Total protein was separated by 10 ~ 12% SDS-PAGE and transferred onto PVDF membranes (Millipore, MA, USA). Following blocking with 5% BSA, the PVDF membranes were incubated with primary antibodies overnight at 4 °C (Supplementary Table 1). This was followed by incubation with anti-mouse/rabbit secondary antibody (Cell signaling technology, Boston, USA) for 45 min at room temperature. The bands were visualized using the ChemiDoc ™ MP Imaging System (BIO-RAD).

Cell proliferation assay

Cell proliferation was assessed under various conditions using Cell Counting kit-8 (CCK-8, Dojindo, Japan) assay according to the manufacturer's instructions. Cells were seeded at a density of 1000 cells per well in 96-well plates, and the optical density (OD) was measured at 450 nm every 24 h for 5 consecutive days. For drug sensitivity detection, 2000 cells were seeded and treated with various drug for 48 h, followed by OD value determination. Three or six duplicates were performed for each group.

Colony formation assay

Cells were seeded into 6-well plates at a density of 700 cells per well and incubated for 48 h. The medium was then replaced with fresh medium containing specific drugs every 3 days. Cells were further cultured approximately 14 days until colonies became visible. Subsequently, the colonies were fixed with 4% paraformaldehyde for 10 min, stained with 0.5% crystal violet, and then counted and photographed.

Cell migration and invasion assay

Transwell migration and invasion assays were conducted using 24-well transwell chambers (Corning, MA, USA) without or with Matrigel. Cells were seeded into the upper chamber in medium supplemented with 2% FBS, while the lower chambers were filled with medium supplemented with 20% FBS. Following a 48-hour incubation period, cells on the upper surface were gently removed using a cotton swab. Subsequently, cells attached to the lower surface were fixed with 4% paraformaldehyde, stained with hematoxylin and eosin (H&E), and then imaged with a microscope.

Wound healing assay

When cells growth in a 6-well plate reached 70 ~ 80%, a 10 μl pipette was used to scratch the cell monolayer. The width of scratches was recorded at various time points using a light microscope. The wound healing percentage was calculated as the migration rate.

Immunofluorescence staining

Cells were fixed with 4% paraformaldehyde for 20 minutes and blocked with 5% BSA for 30 minutes. Following this, cells were incubated with the primary antibodies overnight at 4°C, followed by incubation with fluorescence-labeled secondary antibody at room temperature

for 2 hours. Nuclei were counterstained with 4'-6-diamidino-2-phenylindole (DAPI, Vector labs, USA).

Xenograft tumors model

Female BALB/c-nude mice (4 weeks old), obtained from Vital River Laboratory (Beijing, China), received subcutaneous injection of either HeLa-RPL22L1/vec or HeLa-I-shRPL22L1/control cells into the right dorsal flank (1×10^7 cells in 100 µl PBS). The tumors were measured by vernier caliper, and tumor volume was calculated using the formula: tumor volume = 1/2 length×width^2. For in vivo Sorafenib sensitivity assays, mice bearing HeLa-RPL22L1/vec tumors were randomly divided into two groups: one receiving Sorafenib treatment (30 mg/kg, every 3 days gavage), and others receiving a combination of Sorafenib and Ulixertinib (30 mg/kg, respectively, every 3 days gavage). For in vivo metastasis assay, mice were intravenously injected with 1×10^6 cells of either HeLa-RPL22L1/vec or HeLa-I-shRPL22L1/control. After 7 weeks, the tumor nodules on the lung and liver surfaces were formed and analyzed. Three to five mice were included in each group for each experiment.

Co-immunoprecipitation (Co-IP) assay

Co-IP assay was conducted out using IP Kit (Proteintech, Wuhan, China) following the manufacturer's protocols. Briefly, cells were lysed in cold IP lysis buffer, and soluble lysates were incubated overnight at 4 °C with beads coated with IgG, RPL22L1 or DUSP6 antibodies. Subsequently, western blot analysis was performed to detect the immunoprecipitated proteins.

Statistical analysis

Statistical analysis was performed using SPSS 23.0 software (SPSS Inc. Chicago, IL, USA). The χ^2 test was used to analyze the correlations between RPL22L1 and clinic pathological characteristics. Survival curves were obtained using the Kaplan-Meier method and analyzed with log-rank test. Univariate and multivariate regression analyses were performed using Cox proportional hazards models. Kolmogorov-Smirnov test was used to assess the normal distribution of measurement variables, and ANOVA was employed to confirm homogeneity of variance before applying the two-tailed Student's t-test to compare the significant differences between groups. Data are presented as mean ± SD. Statistical significance was defined as $P < 0.05$.

Results

RPL22L1 is highly expressed in cervical cancer and is associated with poor prognosis

The TCGA database was used to assess the genomic variation of RPL22L1 in cervical cancer. 23% (72/307) of the patients showed RPL22L1 gene variation, including amplification and mRNA differential expression (Supplementary Fig. 1A-B). Subsequently, we examined the mRNA level of RPL22L1 in cervical cancer through TCGA and GEO databases, and found that it is universally highly expressed in cervical cancer compared to non-tumor tissues, with particularly high expression in adenocarcinoma (Fig. 1A-B).

Two sets of cancer cervical tissue microarrays were evaluated for RPL22L1 expression by IHC and RPL22L1 was highly expressed in cervical cancer (Non-tumor vs. Adenocarcinoma: $P = 0.0000$, Non-tumor vs. Squamous cell carcinoma: $P = 0.0019$), with significantly higher levels in adenocarcinoma compared to squamous cell carcinoma ($P = 0.0040$) (Fig. 1C). Moreover, the expression of RPL22L1 protein was significantly associated with histology grade, tumor stage and lymph node metastasis in cervical cancer patients ($P = 0.0043$, 0.0053, 0.0026, respectively) (Fig. 1D). Additional IHC was performed on 130 primary adenocarcinoma patients from our medical center. Consistently, RPL22L1 overexpression was significantly associated with histology grade, tumor stage, recurrence, depth of invasion, vascular space involvement and tumor size ($P = 0.0488$, 0.0198, 0.0294, 0.0000, 0.0068, 0.0016, respectively) (Fig. 1E-F, Supplementary Fig. 1C). Importantly, adenocarcinoma patients with upregulated RPL22L1 exhibit a poorer overall survival (HR = 2.145, $P = 0.0025$) (Fig. 1G). Univariate and multivariate cox regression analysis displayed that RPL22L1 is an independent prognostic factor for overall survival (HR (95%CI) = 0.570 (0.373–0.872), $P = 0.009$; HR (95%CI) = 0.415 (0.232–0.742), $P = 0.003$) (Table 1).

Comparatively, the level of RPL22L1 expression was analyzed in tumorous and non-tumorous counterparts in various cancers using ULCAN database. RPL22L1 exhibited significant overexpression in these cancers including BLCA, BRCA, CESC, CHOL, COAD, ESCA, GBM, HNSC, KIRC, KIRP, LIHC, LUAD, LUSC, PRAD, SARC, SKCM, THCA, THYM, STAD and UCEC (Supplementary Fig. 1D). This suggests that RPL22L1 may act as a carcinogenic modulator.

RPL22L1 promotes the malignant phenotype of cervical cancer cells both in vitro and in vivo

To investigate the impact of RPL22L1 on malignant phenotype of cervical cancer cells, we established a highly invasive HeLa-I cell line derived from adenocarcinoma cell line HeLa using a matrigel-coated transwell chamber. We confirmed its invasiveness through transwell migration and invasion assay (Fig. 2A-B). HeLa-I cells showed elevated RPL22L1 expression and increased cell proliferation compared to parental HeLa cells (Fig. 2C-E).

Subsequently, we established stable overexpression and knockdown of RPL22L1 (shRPL22L1-2) in two squamous cell carcinoma cell lines SiHa and CaSki, as well

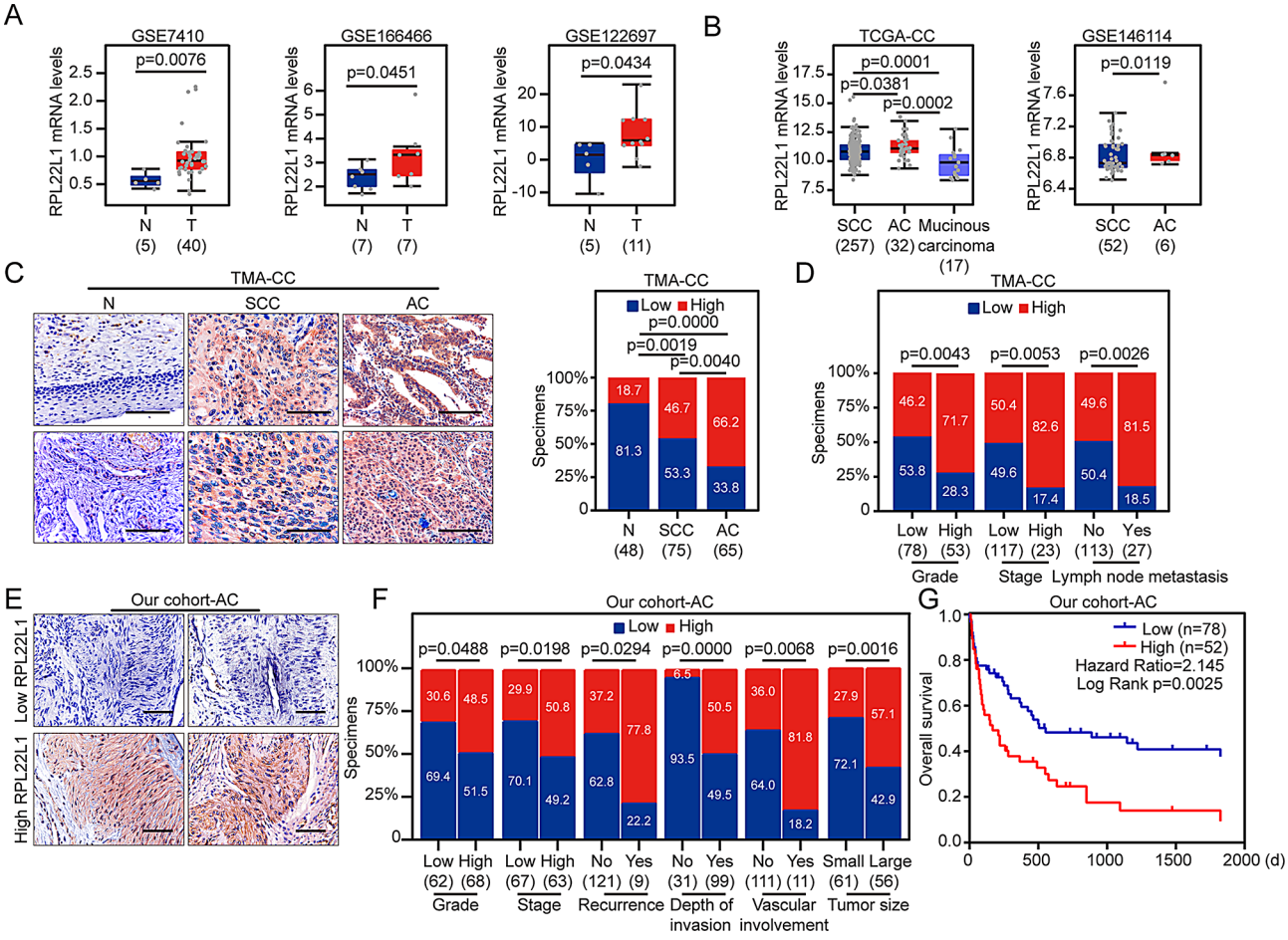

Fig. 1 Expression and prognostic significance of RPL22L1 in cervical cancer. (**A**–**B**) Expression profile of RPL22L1 in cervical cancer based on the TCGA and GEO databases. (**C**) Representative pictures and scoring statistics of RPL22L1 IHC staining in tissue microarrays. Scale bars = 400 μm. (**D**) Scoring statistics of RPL22L1 IHC staining based on clinicopathological parameters on tissue microarrays. (**E**) Representative images of RPL22L1 IHC staining in adenocarcinoma from our center. Scale bars = 100 μm. (**F**) Scoring statistics of RPL22L1 IHC staining in adenocarcinoma based on clinicopathological parameters from our center. (**G**) Overall survival of adenocarcinoma patients from our center. Student's t-test (**A** and **B**), χ^2 test (**C** - **D** and **F**) or Log rank test (**G**). N: Non-tumor tissue. CC: Cervical cancer. SCC: Squamous cell carcinoma. AC: Adenocarcinoma

as Hela (Supplementary Fig. 2A-B). Overexpression of RPL22L1 led to increased cell proliferation, colony formation, migration, and invasion abilities, whereas the opposite effect was observed in RPL22L1 knockdown cells (Fig. 2F-J, Supplementary Fig. 2C-E). To exclude the potential influence of cell proliferation on migration and invasion, the proliferation inhibitor Mitomycin C was used in these assays (Supplementary Fig. 2F). Additionally, RPL22L1 overexpression significantly upregulated the expression of mesenchymal markers N-cadherin and Vimentin, as well as matrix metalloproteinases MMP2 and MMP9. Conversely, RPL22L1 knockdown downregulated the expression of these proteins, while epithelial markers E-cadherin remained unchanged (Fig. 2K). Similar overexpression of N-cadherin and MMP9 in RPL22L1-upregulated cells was observed by an immunofluorescent staining assay (Fig. 2L).

We further investigated the functional role of RPL22L1 in vivo using mouse xenograft models. Overexpression of RPL22L1 significantly promoted tumor growth, as evidenced by increased tumor volume and weight (Fig. 3A-B). In contrast, tumors from RPL22L1 knockdown cells showed limited growth (Fig. 3C-D). Moreover, RPL22L1 expression level was positively correlated with N-cadherin and MMP9 expression, as demonstrated by IHC staining and western blot analysis (Fig. 3E-F). In the metastatic xenograft tumor model established by tail vein injection, RPL22L1-overexpressing cells formed more metastatic nodules on the liver and lung surfaces compared to the control group (Fig. 3G). Conversely, RPL22L1 knockdown resulted in fewer metastatic nodules (Fig. 3H). Overall, RPL22L1 enhanced the malignancy of cervical cancer both in vitro and in vivo.

Table 1 Univariate and multivariate Cox regression analysis of different prognosis factors in cervical cancer

Factors	Cases	Univariate analysis[a]		Multivariate analysis[a]	
		HR (95%CI)	*P* value[b]	HR (95%CI)	*P* value[b]
Total	130				
RPL22L1 expression		0.570 (0.373–0.872)	**0.009**	0.415 (0.232–0.742)	**0.003**
Low expression	78				
High expression	52				
Age		0.907 (0.599–1.372)	0.644		
<47	69				
≥47	61				
Grade		6.843 (4.135–11.324)	**0.000**	0.267(1.125–0.572)	**0.001**
I/II	62				
III	68				
Tumor size (cm3)		1.492 (0.430–1.044)	0.075	1.872 (1.127–3.107)	**0.015**
≤5	61				
>5	56				
Stage		5.550 (3.379–9.113)	**0.000**	5.974 (1.402–25.454)	0.067
I	67				
II	63				
Metastasis		1.315 (0.731–2.367)	0.345		
Negative	110				
Positive	20				
Vascular space involvement		1.566 (0.683–3.591)	0.289		
No	111				
Yes	11				
Depth of cervical stromal invasion		0.650 (0.403–1.048)	0.077	1.273 (0.645–2.510)	0.487
<1/2	31				
≥1/2	99				
Recurrence		0.156 (0.038–0.673)	**0.000**	5.974 (1.402–25.454)	**0.016**
Negative	121				
Positive	9				

[a]Cox regression model. [b]Log-rank test

RPL22L1 activates ERK to promote cervical cancer malignancy

We utilized the LinkedOmics database to identify genes positively or negatively related to RPL22L1 (FDR < 0.01) (Supplementary Fig. 3A). Gene Set Enrichment Analysis (GSEA) and Over-Representation Analysis (ORA) revealed that RPL22L1-related genes are involved in MAP kinase phosphatase activity (Supplementary Fig. 3B-C). Consistently, similar results were obtained from entering RPL22L1-related genes from the Genecards database into BiNGO (Supplementary Fig. 3D). Western blotting of overexpressing RPL22L1 cells showed increased phosphorylated MEK, ERK, and S6K, as well as c-Myc expression, whereas RPL22L1 knockdown reversed these changes. In contrast, the levels of p38 and JNK remained unaffected (Fig. 4A). These results were consistent with those obtained from western blot analysis of xenograft tumors (Fig. 4B). Additionally, immunofluorescent staining demonstrated increased p-ERK in RPL22L1-overexpressing cells (Supplementary Fig. 3E).

Next, we used specific inhibitors of MEK (U0126) and ERK (Ulixertinib and SCH772984) to evaluate whether they can block cell growth in RPL22L1-overexpressed tumor cells. Both ERK inhibitors induced a dose-dependent suppression of c-Myc expression, although Ulixertinib caused a paradoxical increase in p-ERK levels (Supplementary Fig. 3F). Additionally, ERK inhibition reduced the expression of MMP9 and N-cadherin, as well as inhibited colony growth, cell viability, migration, and invasion (Fig. 4C-G). In contrast, the MEK inhibitor U0126 only partially blocked ERK activation and did not affect colony growth, cell viability, migration, or invasion (Supplementary Fig. 4A-E). These data support the conclusion that RPL22L1 promotes tumor aggression primarily through ERK signaling.

RPL22L1 interacts and inhibits the dephosphorylation of DUSP6 to activate ERK

We conducted an overlap analysis between MAPK/ERK pathway-related genes from MSigDB database and RPL22L1-interacting proteins from BioGRID database and discovered DUSP6 and PTPRR as potential interacting partners (Fig. 5A, Supplementary Fig. 5A). Notably, DUSP6 is a dual-specific phosphatase known to bind and specifically dephosphorylate ERK [16, 17]. Analysis of the TCGA database revealed no significant correlation between RPL22L1 expression and DUSP6 expression (Supplementary Fig. 5B). GeneMANIA revealed that RPL22L1 binds to DUSP6 to activate ERK (Supplementary Fig. 5C). Furthermore, protein-protein docking further demonstrated that DUSP6 forms a stable bond with RPL22L1, involving ARG65 of DUSP6 and GLU117 of RPL22L1, yielding a PIPER pose energy of approximately −790.981 kcal/mol (Fig. 5B).

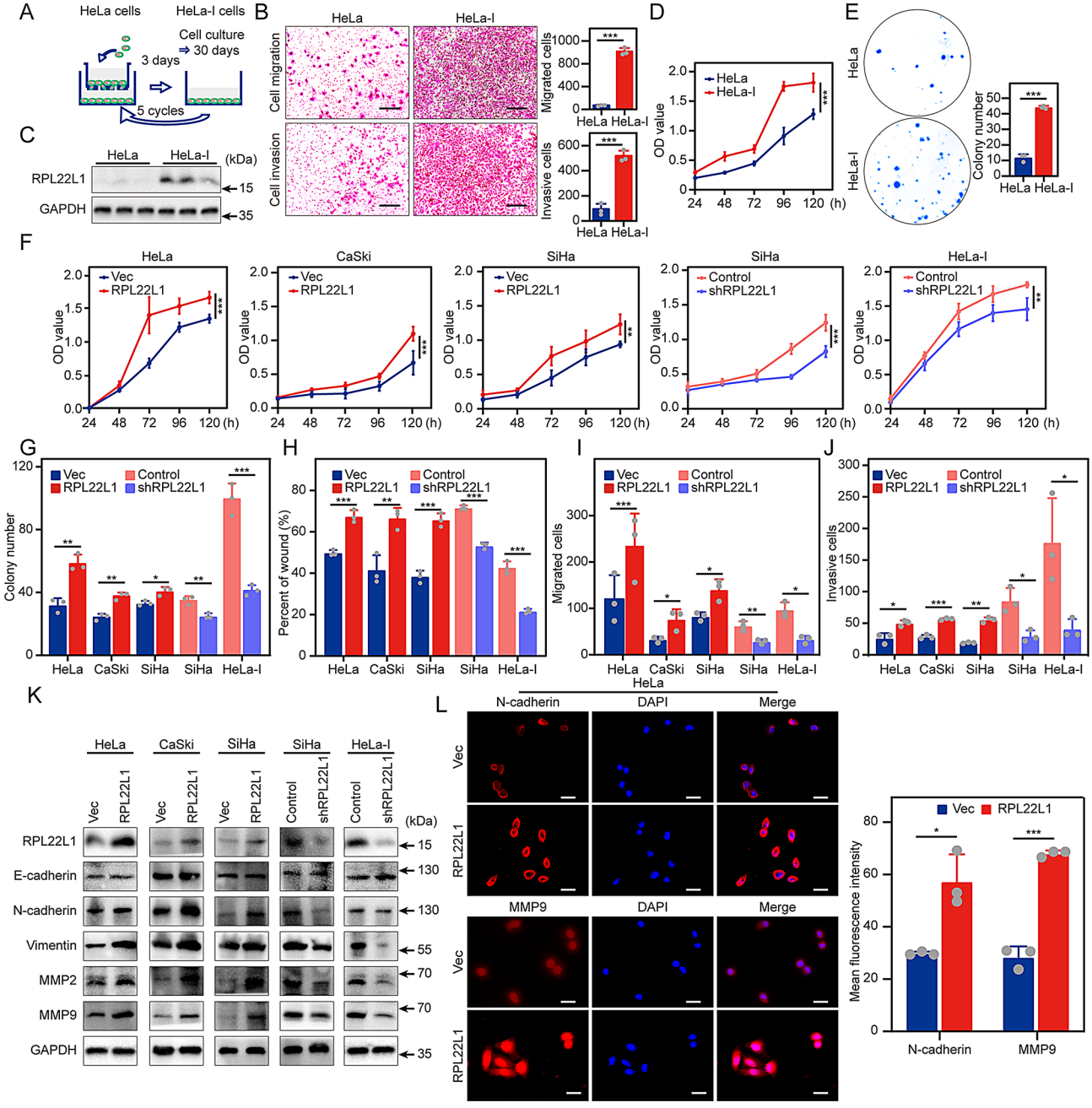

Fig. 2 The effect of RPL22L1 on malignant features of cervical cancer cells in vitro. (**A**) HeLa-I cells with high invasiveness were isolated through multiple selections with transwell assay. (**B**) The high invasiveness of HeLa-I cells was confirmed using transwell assays ($N=3$). Scale bars = 500 μm. (**C**) The expression of RPL22L1 in HeLa-I cells was significantly higher than that in parental HeLa cells. (**D**–**E**) Highly invasive HeLa-I cells showed increased cell viability and colony growth ability compared to parental HeLa cells, as indicated by CCK-8 ($N=6$) (**D**) and colony formation assay ($N=3$) (**E**). (**F**–**J**) CCK-8 assays ($N=6$) (**F**), colony formation assays ($N=3$) (**G**), wound-healing assays ($N=3$) (**H**), transwell migration ($N=3$) (**I**) and invasion assays ($N=3$) (**J**) of cells with RPL22L1 overexpression or knockdown. Scale bars = 500 μm. (**K**) Western blots of EMT-related proteins. (**L**) Immunofluorescence staining and statistical analysis for MMP9 and N-cadherin expression ($N=3$). Scale bars = 20 μm. Data are presented as the mean ± SD. Student's t-test. * $P<0.05$, ** $P<0.01$, *** $P<0.001$

A Co-IP assay was performed and the interaction between DUSP6 and RPL22L was confirmed (Fig. 5C). Knockdown of RPL22L1 significantly increased the interaction between DUSP6 and ERK, resulting in decreased p-ERK (Fig. 5D). Knockdown of DUSP6 increased p-ERK and alleviated the inhibitory effect of RPL22L1 knockdown on p-ERK, N-cadherin, MMP9 and c-Myc expression, as well as cell proliferation, migration, and invasion (Fig. 5E-I). Overall, these data suggest that RPL22L1 contributes to cell malignant characteristics by disrupting

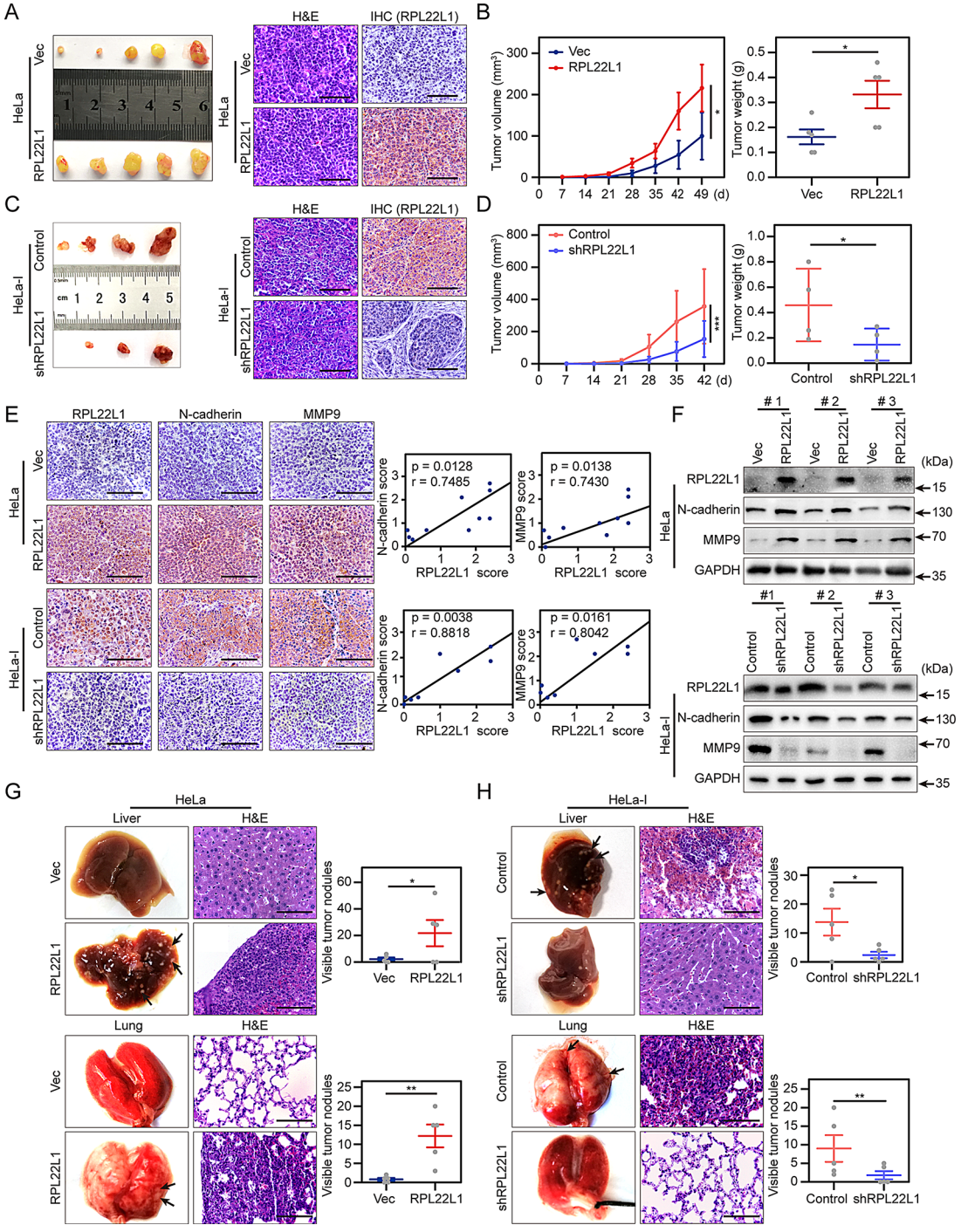

Fig. 3 The effect of RPL22L1 on tumorigenesis and metastasis of cervical cancer in vivo. (**A**–**D**) Gross view of transplanted tumors formed by RPL22L1-overexpresssing ($N=5$) (**A**) or knockdown ($N=4$) (**C**) cells. The representative images for H&E staining and RPL22L1 IHC staining of transplanted tumor. Scale bars = 400 μm. Volumes and weights of tumor were measured. (**E**–**F**) IHC staining (**E**) and western blots (**F**) of subcutaneous tumors. Pearson's correlation between the expression of RPL22L1 and EMT-related proteins was analyzed based on IHC staining. Scale bars = 400 μm. (**G**–**H**) Representative images and H&E staining of liver and lung metastatic nodules, and metastatic nodules were counted ($N=5$). Scale bars = 400 μm. Data are presented as the mean ± SD. Student's t-test. $^{*}P<0.05$, $^{**}P<0.01$, $^{***}P<0.001$

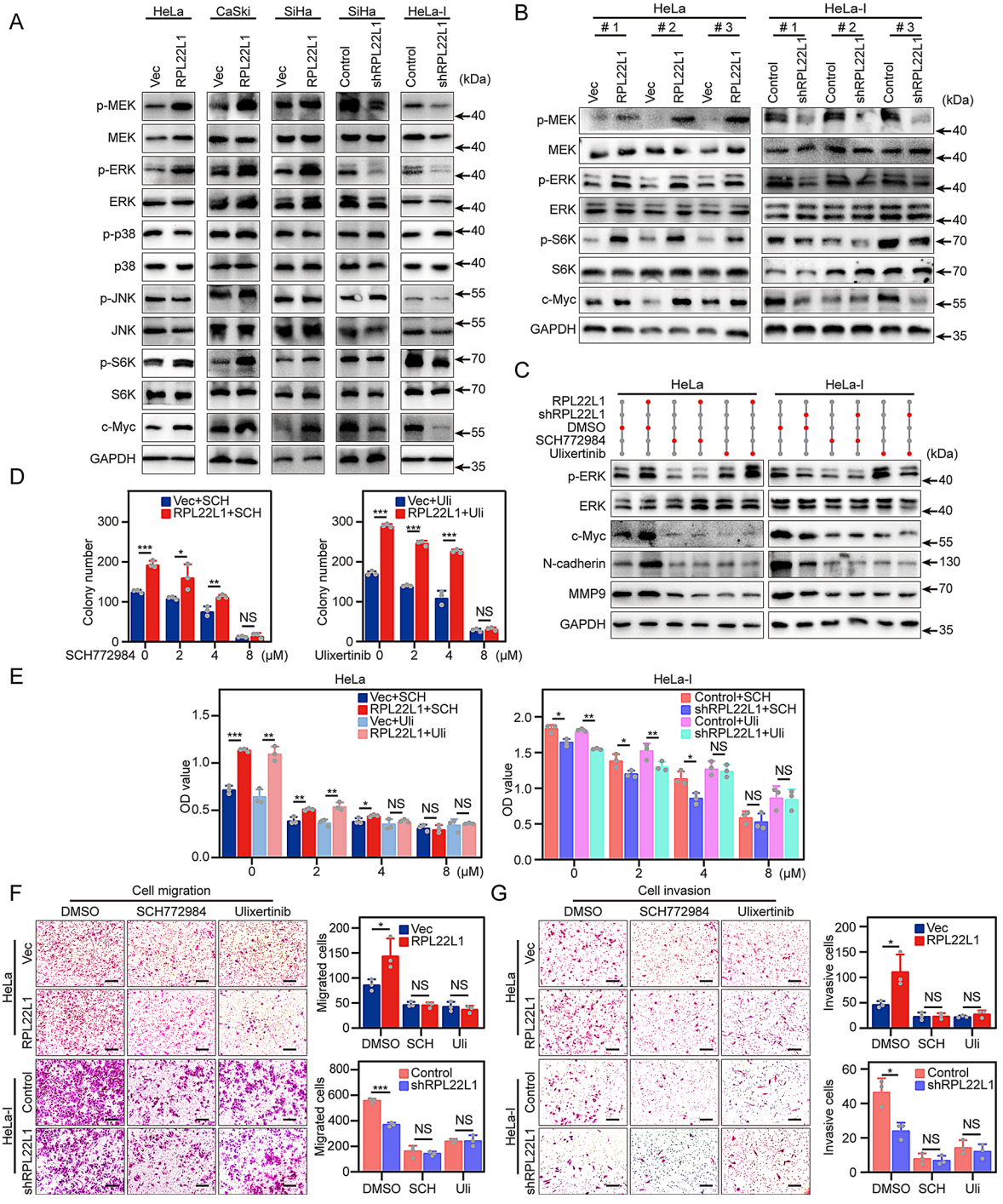

Fig. 4 RPL22L1 overexpression leads to ERK activation. (**A**) Western blots for the expression of MAPK pathway-associated molecules. (**B**) Western blotting analysis of MEK-ERK pathway-related protein in transplanted tumors. (**C**) Western blots revealing the effects of ERK inhibitor on cells. (**D**) Colony growth of cells after treatment with different concentrations of ERK inhibitor ($N=3$). (**E**) CCK-8 assays showing the dose-dependent suppressive effect of ERK inhibitor on cells viability ($N=3$). (**F**–**G**) Transwell assays showing the effect of ERK inhibitor on RPL22L1-promoted cells migration and invasion ($N=3$). Scale bars = 200 μm. Data are presented as the mean ± SD. Student's t-test. NS Non-significance, $^{*}P<0.05$, $^{**}P<0.01$, $^{***}P<0.001$

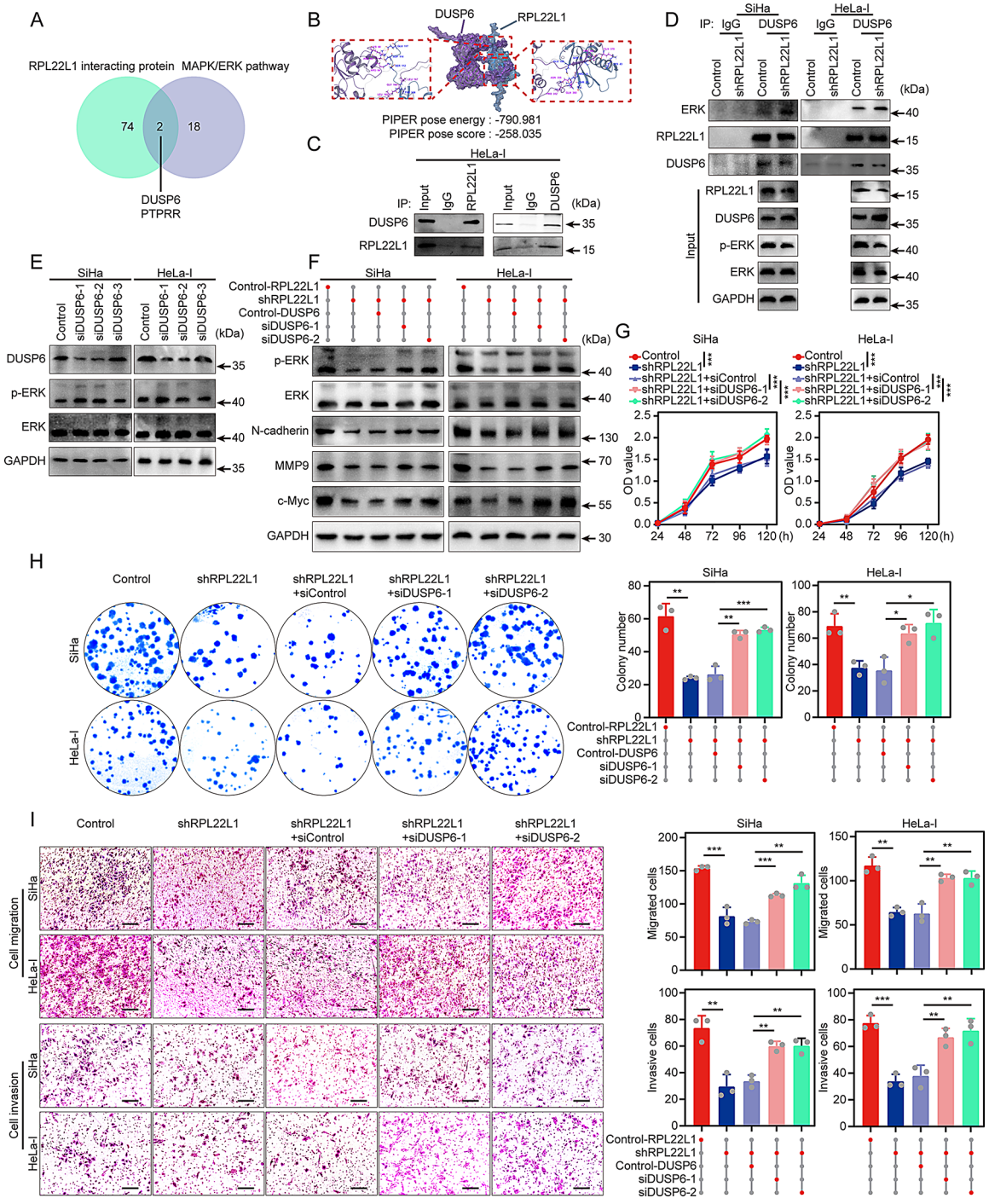

Fig. 5 RPL22L1 interacts with DUSP6 to promote ERK activation. (**A**) Venn plot showing the potential interacting partner for RPL22L1-regulated ERK. (**B**) Protein-protein docking of DUSP6 and RPL22L1. (**C**–**D**) Co-IP assay showing the interaction between RPL22L1 and DUSP6. (**E**–**F**) Western blots revealing the effects of DUSP6 knockdown on cells. (**G**–**I**) CCK-8 (**G**), clone formation (**H**) and transwell (**I**) assays revealing the effects of DUSP6 knockdown on cells ($N = 3$). Scale bars = 500 μm. Data are presented as the mean ± SD. Student's t-test. NS Non-significance, $^{*}P < 0.05$, $^{**}P < 0.01$, $^{***}P < 0.001$

the interaction between ERK and DUSP6, thus enhancing ERK activation.

The combined application of ERK inhibitors with Sorafenib can effectively inhibit cervical cancer cells with high RPL22L1 expression both in vivo and in vitro

Sorafenib is a multi-kinase inhibitor and specifically inhibits RAF upstream of ERK. We evaluated the response to Sorafenib in cervical cancer in vitro and in vivo. Overexpression of RPL22L1 resulted in decreased Sorafenib sensitivity, as indicated by significantly elevated IC50 and colony growth, while knockdown of RPL22L1 showed the opposite effect (Fig. 6A-B). Sorafenib failed to suppress the expression levels of p-MEK, p-ERK, p-S6K, c-Myc, and N-cadherin in RPL22L1-overexpressing cells. Moreover, RPL22L1 overexpression significantly reduced cleaved caspase 3 expression while elevating levels of Bcl2 and Bcl-xL during Sorafenib treatment. Conversely, RPL22L1 knockdown exerted the opposite effect on the expression of these proteins. Combination of Sorafenib and ERK inhibitor effectively counteracted these molecular changes in RPL22L1-upregulated cells, despite an increase in p-MEK levels (Fig. 6C). Furthermore, the combination with ERK inhibitor significantly decreased the IC50 of Sorafenib and synergistically inhibited the proliferation, migration, and invasion in RPL22L1-upregulated cells (Fig. 6D-H, Supplementary Fig. 6A-C). However, U0126 did not enhance the therapeutic efficacy of Sorafenib in RPL22L1-upregulated cells (Fig. 6C-H, Supplementary Fig. 6A-C).

We performed in vivo validation using Sorafenib and the first-in-class oral ERK inhibitor Ulixertinib. Sorafenib alone did not reduce the volume or weight of xenograft tumors formed by RPL22L1-upregulated cells. However, the combination of Sorafenib and Ulixertinib significantly suppressed tumor growth (Fig. 6I). These results highlight that RPL22L1 limits the effectiveness of Sorafenib by modulating ERK activity and suggest that combination therapy with ERK inhibitors and Sorafenib could be a promising strategy for patients with elevated RPL22L1 levels (Fig. 7).

Discussion

Adenocarcinoma and squamous cell carcinoma of cervix are the two major histology types of cervical cancer. While extensive research on oncogenesis and malignant mechanisms of cervical squamous cell carcinoma has led to a decrease in its incidence, few studies have focused on women with adenocarcinoma and effective biomarkers for this subtype remain elusive [3]. In this study, we demonstrate that RPL22L1 is universally highly expressed in both cervical adenocarcinoma and squamous cell carcinoma, and promotes tumor malignancy by activating ERK. Our finding has made it possible for RPL22L1 to serve as a universal biomarker, as well as an indicator of ERK inhibitor combination therapy in cervical cancer.

This study provides substantial evidence supporting the crucial role of RPL22L1 in the malignant progression of cervical cancer. Our initial analysis of public databases revealed that RPL22L1 is universally expressed at high level in a significant portion of cervical cancer cases, especially in adenocarcinoma cases. This finding was further validated by the evaluation of primary cervical cancer tissues using both commercial tissue microarrays and surgical samples from our medical center. Statistical analysis confirmed that RPL22L1 overexpression is associated with histology grade, clinical stage, size, recurrence, vascular space involvement, and overall survival. Univariate and multivariate Cox regression analysis identify RPL22L1 as an independent predictor of adverse outcomes in adenocarcinoma patients. Our current understanding of the carcinogenesis and malignant progression of adenocarcinoma is still limited. These data suggest that RPL22L1 may be an important oncogene with crucial function not only in squamous cell carcinoma but also with greater implications in adenocarcinoma.

The role of RPL22L1 in cervical cancer tumorigenesis was demonstrated via both in vitro cell models and in vivo animal studies. Cervical cancer cells with RPL22L1 overexpression showed increased proliferation, migration, invasion, and metastasis. Conversely, downregulation of RPL22L1 in these cells reversed these aggressive phenotypes. Additionally, RPL22L1 overexpression resulted in elevated levels of MMP9, N-cadherin, and c-Myc, all critical downstream targets of ERK and key regulators of EMT. Co-IP assays revealed a direct interaction between RPL22L1 and DUSP6, a phosphatase that dephosphorylates and inactivates ERK. Thus, overexpression of RPL22L1 leads to ERK activation by sequestering DUSP6 away from ERK. These findings likely explain the enhanced malignant properties observed in cervical cancer cells with high RPL22L1 levels.

Current standard therapies for advanced cervical cancer, including chemotherapy and radiotherapy, often yield limited results. Sorafenib, an FDA-approved drug for various cancers such as hepatocellular carcinoma [13], renal cell carcinoma [14], and thyroid cancer [16], is being explored in clinical trials for cervical cancer, often in combination with other therapies. Some trials have shown promise, although results remain preliminary. Our study identified a synergistic effect between ERK inhibitors and Sorafenib in RPL22L1-overexpressed cervical cancer both in *vitro* and in vivo models. MEK-ERK activation is prevalent in many tumors and is a well-established signaling pathway involved in tumorigenesis [31]. Anti-tumor strategies targeting the MEK-ERK pathway are a major area of research interest, with

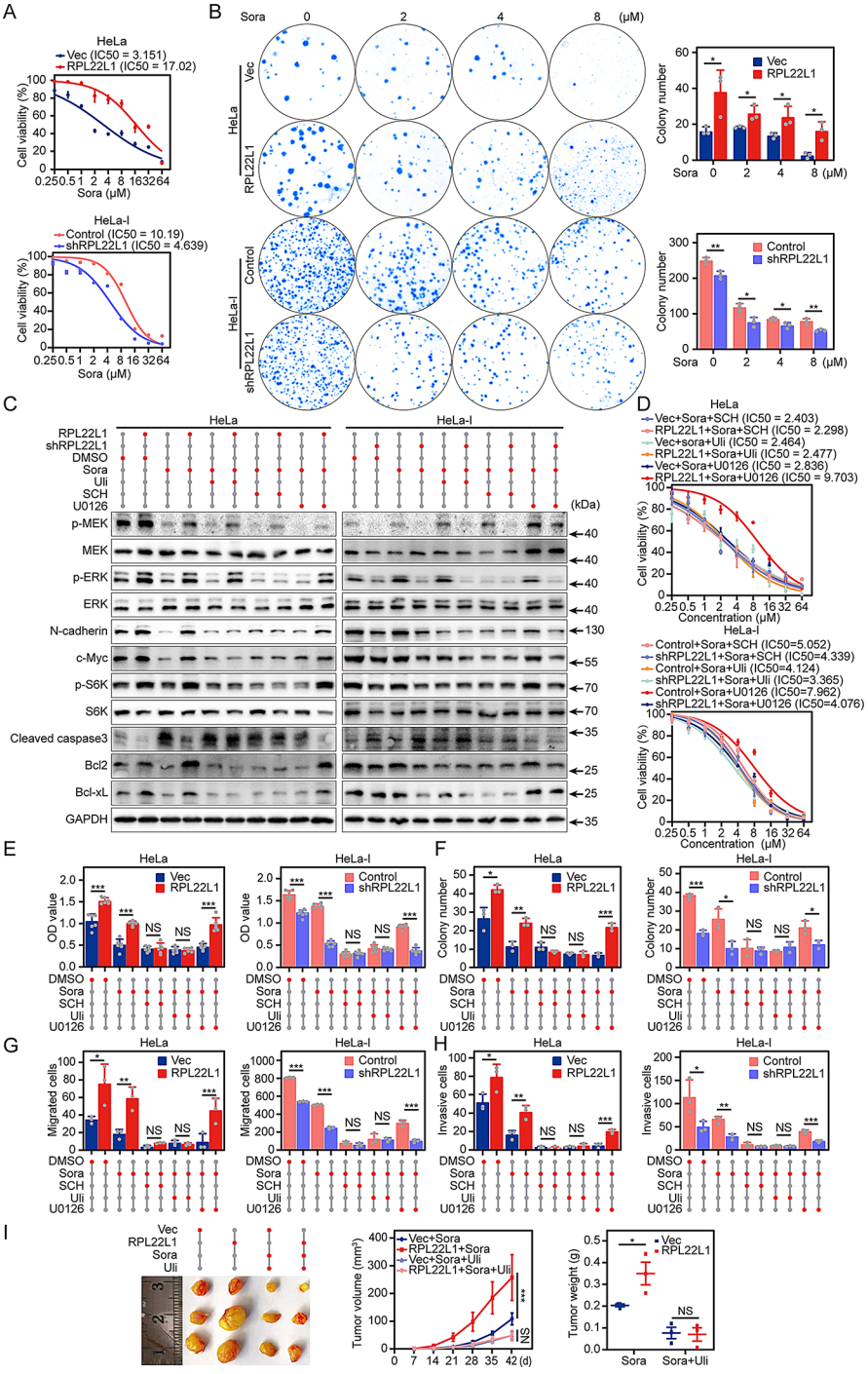

Fig. 6 The combined application of ERK inhibitors mitigates RPL22L1 overexpressing cervical cancer cells. (**A**) CCK-8 assays determining the IC50 of Sorafenib ($N=3$). (**B**) Colony formation assays showing dose-dependent effect of Sorafenib on cells colony growth ($N=3$). (**C**) Western blots revealing the effect of Sorafenib alone, or combined with three different inhibitors on cells. (**D**) CCK-8 assays showing the IC50 of Sorafenib combined with three different inhibitors ($N=3$). (**E**–**H**) CCK-8 (**E**), colony formation (**F**) and transwell (**G**, **H**) assays showing the effect of Sorafenib alone, or combined with three different inhibitors on cells ($N=3$). (**I**) Gross view of tumors following treatment with Sorafenib alone or combined with Ulixertinib. Tumor volumes and weights were measured ($N=3$). Data are presented as the mean ± SD. Student's t-test. NS Non-significance, * $P<0.05$, ** $P<0.01$, *** $P<0.001$

several ERK inhibitors currently undergoing clinical trials [32]. Based on our findings, a RPL22L1-biomarker-based combination therapy using ERK inhibitors and Sorafenib merits further investigation in clinical settings of cervical cancer. In our previous studies on hepatocellular carcinoma, RPL22L1 was also found to specifically activate the ERK pathway [22]. Additionally, RPL22L1 can also activate STAT3 pathway in gliomas and PI3K/AKT/mTOR

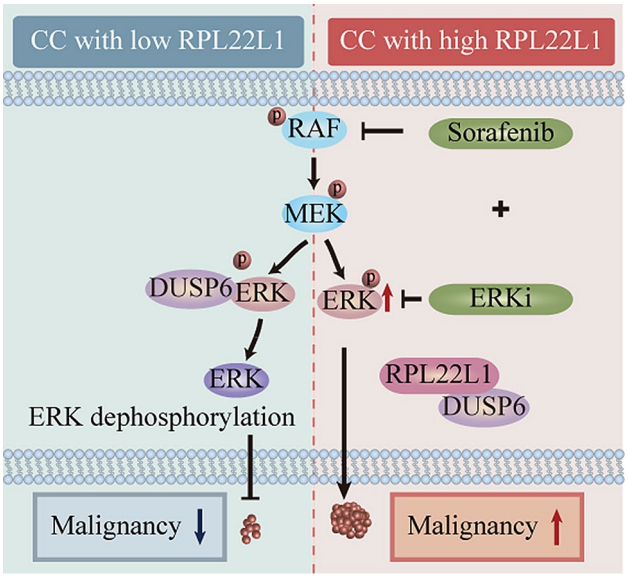

Fig. 7 Schematic illustration of RPL22L1 regulating cervical cancer malignancy via DUSP6-ERK axis

pathway in prostate cancer [23, 33]. Therefore, there may be different combination therapy strategies in various cancer types. In future studies we will explore other targets modulated by RPL22L1 and evaluate potential combination therapy strategies in different cancer types.

In conclusion, our study demonstrates that RPL22L1 plays a crucial role in cervical cancer progression by enhancing ERK signaling. RPL22L1 may serve as a universal marker for both cervical adenocarcinoma and squamous cell carcinoma, and a promising indicator to guide ERK inhibitor combination therapy.

Abbreviations

RPL22L1	Ribosomal L22-like 1
EMT	Epithelial-to-mesenchymal transition
H&E	Hematoxylin and eosin
ERK	Extracellular regulated protein kinase
MEK	Mitogen-activated protein kinase kinase
DUSP6	Dual-specificity phosphatase 6
JNK	c-Jun N-terminal kinase
MAPK	Mitogen-activated protein kinase
TCGA	The Cancer Genome Atlas
GEO	Gene Expression Omnibus
GSEA	Gene set enrichment analysis
ORA	Over-Representation Analysis
IHC	Immunohistochemistry

Supplementary Information

The online version contains supplementary material available at https://doi.org/10.1186/s12967-025-06249-0.

Supplementary Material 1

Supplementary Material 2

Acknowledgements

Not applicable.

Author contributions

YJ, DZ, and NW designed and supervised the study; DZ performed the most of experiments; CZ, MZ and SX performed the data analysis; YZ and SN took charge of bioinformatics analyses; PJ participated in functional assays; XY was engaged in animal investigations; HM collected the clinical samples; DS, GJ, and YM provided technique supports; DZ, XC, and SX drafted and embellished the manuscript; YJ, DZ, and NW acquired funding to support this work.

Funding

This work was supported by the National Natural Science Foundation of China (No. 82172353, 81802428), Natural Science Foundation of Heilongjiang Province (No. ZD2023H002), China Postdoctoral Science Foundation (No. 2020T130159, 2024MD753939, GZC20230649), Education Department of Heilongjiang Province (LJGXCG2024-P12), and Heilongjiang Touyan Innovation Team Program.

Data availability

Data is available on request from corresponding authors.

Declarations

Ethics approval and content to participate

This study was approved by the Ethics Committee of Harbin Medical University (No. HMUIRB20150023, Harbin, China). Animal experiments were approved by the Institutional Animal Review Board of Harbin Medical University. All patients included in the study provided informed consent.

Consent for publication

Not applicable.

Competing interests

The authors disclose no potential conflict of interest.

Received: 16 November 2024 / Accepted: 11 February 2025
Published online: 28 February 2025

References

1. Siegel RL, Miller KD, Fuchs HE, Jemal A. Cancer statistics, 2022. CA Cancer J Clin. 2022;72:7–33.
2. Sung H, Ferlay J, Siegel RL, Laversanne M, Soerjomataram I, Jemal A, Bray F. Global Cancer statistics 2020: GLOBOCAN estimates of incidence and Mortality Worldwide for 36 cancers in 185 countries. CA Cancer J Clin. 2021;71:209–49.
3. Lee YY, Choi CH, Kim TJ, Lee JW, Kim BG, Lee JH, Bae DS. A comparison of pure adenocarcinoma and squamous cell carcinoma of the cervix after radical hysterectomy in stage IB-IIA. Gynecol Oncol. 2011;120:439–43.
4. Smith AJB, Beavis AL, Rositch AF, Levinson K. Disparities in diagnosis and treatment of cervical adenocarcinoma compared with squamous cell carcinoma: an analysis of the National Cancer Database, 2004–2017. J Lower Genit Tract Dis. 2023;27:29–34.
5. Abu-Rustum NR, Yashar CM, Arend R, Barber E, Bradley K, Brooks R, Campos SM, Chino J, Chon HS, Crispens MA, et al. NCCN Guidelines(R) insights: Cervical Cancer, Version 1.2024. J Natl Compr Canc Netw. 2023;21:1224–33.
6. Liontos M, Kyriazoglou A, Dimitriadis I, Dimopoulos M-A, Bamias A. Systemic therapy in cervical cancer: 30 years in review. Crit Rev Oncol/Hematol. 2019;137:9–17.
7. Lee J, Lin J-B, Sun F-J, Chen Y-J, Chang C-L, Jan Y-T, Wu M-H. Safety and efficacy of semiextended field intensity-modulated radiation therapy and concurrent cisplatin in locally advanced cervical cancer patients. Medicine. 2017;96.
8. Zheng M, Huang L, He L, Ding H, Wang HY, Zheng LM. Evaluation of the effects of type II radical hysterectomy in the treatment of 960 patients with stage IB–IIB cervical carcinoma: a retrospective study. J Surg Oncol. 2010;103:435–41.
9. del Campo JM, Prat A, Gil-Moreno A, Perez J, Parera M. Update on novel therapeutic agents for cervical cancer. Gynecol Oncol. 2008;110:S72–76.
10. Wan PK, Leung TH, Siu MK, Mo XT, Tang HW, Chan KK, Cheung AN, Ngan HY. HPV-induced Nurr1 promotes cancer aggressiveness, self-renewal, and

radioresistance via ERK and AKT signaling in cervical cancer. Cancer Lett. 2021;497:14–27.
11. Rasi Bonab F, Baghbanzadeh A, Ghaseminia M, Bolandi N, Mokhtarzadeh A, Amini M, Dadashzadeh K, Hajiasgharzadeh K, Baradaran B, Bannazadeh Baghi H. Molecular pathways in the development of HPV-induced cervical cancer. EXCLI J. 2021;20:320–37.
12. Zhao A, Pan Y, Gao Y, Zhi Z, Lu H, Dong B, Zhang X, Wu M, Zhu F, Zhou S, Ma S. MUC1 promotes cervical squamous cell carcinoma through ERK phosphorylation-mediated regulation of ITGA2/ITGA3. BMC Cancer. 2024;24:559.
13. Palmer P DH. Sorafenib in advanced hepatocellular carcinoma. N Engl J Med. 2008;359:2498–2499.
14. Escudier B, Eisen T, Stadler WM, Szczylik C, Oudard S, Siebels M, Negrier S, Chevreau C, Solska E, Desai AA, et al. Sorafenib in advanced clear-cell renal-cell carcinoma. N Engl J Med. 2007;356:125–34.
15. Thota R, Johnson DB, Sosman JA. Trametinib in the treatment of melanoma. Expert Opin Biol Ther. 2015;15:735–47.
16. Boucai L, Zafereo M, Cabanillas ME. Thyroid Cancer: Rev JAMA. 2024;331:425–35.
17. He Y, Luo Y, Huang L, Zhang D, Wang X, Ji J, Liang S. New frontiers against sorafenib resistance in renal cell carcinoma: from molecular mechanisms to predictive biomarkers. Pharmacol Res. 2021;170.
18. Ingram K, Samson SC, Zewdu R, Zitnay RG, Snyder EL, Mendoza MC. NKX2-1 controls lung cancer progression by inducing DUSP6 to dampen ERK activity. Oncogene. 2021;41:293–300.
19. Courtney TM, Deiters A. Optical control of protein phosphatase function. Nat Commun. 2019;10:4384.
20. Pecoraro A, Pagano M, Russo G, Russo A. Ribosome biogenesis and cancer: overview on ribosomal proteins. Int J Mol Sci. 2021;22.
21. Wu N, Wei J, Wang Y, Yan J, Qin Y, Tong D, Pang B, Sun D, Sun H, Yu Y, et al. Ribosomal L22-like1 (RPL22L1) promotes ovarian Cancer metastasis by inducing epithelial-to-mesenchymal transition. PLoS ONE. 2015;10:e0143659.
22. Zhang D, Zhou Y, Ma Y, Jiang P, Lv H, Liu S, Mu Y, Zhou C, Xiao S, Ji G, et al. Ribosomal protein L22-like1 (RPL22L1) mediates sorafenib sensitivity via ERK in hepatocellular carcinoma. Cell Death Discov. 2022;8:365.
23. Chen Y, Mu Y, Guan Q, Li C, Zhang Y, Xu Y, Zhou C, Guo Y, Ma Y, Zhao M, et al. RPL22L1, a novel candidate oncogene promotes temozolomide resistance by activating STAT3 in glioblastoma. Cell Death Dis. 2023;14:757.
24. Rao S, Peri S, Hoffmann J, Cai KQ, Harris B, Rhodes M, Connolly DC, Testa JR, Wiest DL. RPL22L1 induction in colorectal cancer is associated with poor prognosis and 5-FU resistance. PLoS ONE. 2019;14:e0222392.
25. Liang Z, Mou Q, Pan Z, Zhang Q, Gao G, Cao Y, Gao Z, Pan Z, Feng W. Identification of candidate diagnostic and prognostic biomarkers for human prostate cancer: RPL22L1 and RPS21. Med Oncol. 2019;36:56.
26. Qin X, Liu Z, Yan K, Fang Z, Fan Y. Integral analysis of the RNA binding protein-associated Prognostic Model for Renal Cell Carcinoma. Int J Med Sci. 2021;18:953–63.
27. Bell JL, Hagemann S, Holien JK, Liu T, Nagy Z, Schulte JH, Misiak D, Huttelmaier S. Identification of RNA-binding proteins as targetable putative oncogenes in neuroblastoma. Int J Mol Sci. 2020;21.
28. Oughtred R, Stark C, Breitkreutz B-J, Rust J, Boucher L, Chang C, Kolas N, O'Donnell L, Leung G, McAdam R, et al. The BioGRID interaction database: 2019 update. Nucleic Acids Res. 2019;47:D529–41.
29. Warde-Farley D, Donaldson SL, Comes O, Zuberi K, Badrawi R, Chao P, Franz M, Grouios C, Kazi F, Lopes CT, et al. The GeneMANIA prediction server: biological network integration for gene prioritization and predicting gene function. Nucleic Acids Res. 2010;38:W214–20.
30. Shannon P, Markiel A, Ozier O, Baliga NS, Wang JT, Ramage D, Amin N, Schwikowski B, Ideker T. Cytoscape: a Software Environment for Integrated Models of Biomolecular Interaction Networks. Genome Res. 2003;13:2498–504.
31. Guo YJ, Pan WW, Liu SB, Shen ZF, Xu Y, Hu LL. ERK/MAPK signalling pathway and tumorigenesis. Exp Ther Med. 2020;19:1997–2007.
32. Kidger AM, Munck JM, Saini HK, Balmanno K, Minihane E, Courtin A, Graham B, O'Reilly M, Odle R, Cook SJ. Dual-mechanism ERK1/2 inhibitors exploit a distinct binding Mode to Block Phosphorylation and Nuclear Accumulation of ERK1/2. Mol Cancer Ther. 2020;19:525–39.
33. Yi X, Zhang C, Liu B, Gao G, Tang Y, Lu Y, Pan Z, Wang G, Feng W. Ribosomal protein L22-like1 promotes prostate cancer progression by activating PI3K/Akt/mTOR signalling pathway. J Cell Mol Med. 2023;27:403–11.

Publisher's note